State-dependent and site-directed photodynamic transformation of HCN2 channel by singlet oxygen

Weihua Gao, Zhuocheng Su, Qinglian Liu, and Lei Zhou

Department of Physiology and Biophysics, School of Medicine, Virginia Commonwealth University, Richmond, VA 23298

Singlet oxygen ($^1O_2$), which is generated through metabolic reactions and oxidizes numerous biological molecules, has been a useful tool in basic research and clinical practice. However, its role as a signaling factor, as well as a mechanistic understanding of the oxidation process, remains poorly understood. Here, we show that hyperpolarization-activated, cAMP-gated (HCN) channels–which conduct the hyperpolarization-activated current (I_h) and the voltage-insensitive instantaneous current (I_{inst}), and contribute to diverse physiological functions including learning and memory, cardiac pacemaking, and the sensation of pain–are subject to modification by $^1O_2$. To increase the site specificity of $^1O_2$ generation, we used fluorescein-conjugated cAMP, which specifically binds to HCN channels, or a chimeric channel in which an in-frame $^1O_2$ generator (SOG) protein was fused to the HCN C terminus. Millisecond laser pulses reduced I_h current amplitude, slowed channel deactivation, and enhanced I_{inst} current. The modification of HCN channel function is a photodynamic process that involves $^1O_2$, as supported by the dependence on dissolved oxygen in solutions, the inhibitory effect by a $^1O_2$ scavenger, and the results with the HCN2-SOG fusion protein. Intriguingly, $^1O_2$ modification of the HCN2 channel is state dependent: laser pulses applied to open channels mainly slow down deactivation and increase I_{inst}, whereas for the closed channels, $^1O_2$ modification mainly reduced I_h amplitude. We identified a histidine residue (H434 in S6) near the activation gate in the pore critical for $^1O_2$ modulation of HCN function. Alanine replacement of H434 abolished the delay in channel deactivation and the generation of I_{inst} induced by photodynamic modification. Our study provides new insights into the instantaneous current conducted by HCN channels, showing that modifications to the region close to the intracellular gate underlie the expression of I_{inst}, and establishes a well-defined model for studying $^1O_2$ modifications at the molecular level.

The Journal of General Physiology

INTRODUCTION

Molecular oxygen has three different electron configurations: the triplet ground state ($^3\Sigma$), and the first and second singlet excited states ($^1\Delta$ and $^1\Sigma$) (Kochevar, 2004; Ogilby, 2010). Singlet oxygen ($^1O_2$) mainly refers to the $^1\Delta$ state because of its longer lifetime compared with the $^1\Sigma$ state. $^1O_2$ is highly reactive and oxidizes a wide range of biomolecules including DNA, proteins, and unsaturated lipids. Among the 20 amino acids, $^1O_2$ mainly reacts with histidine, cysteine, methionine, tyrosine, and tryptophan (Gracanin et al., 2009). Histidine is an effective quencher of $^1O_2$ and the major target of $^1O_2$ oxidation. Under physiological conditions, $^1O_2$ can be generated through metabolic reactions and functions as a signaling factor, such as in plants and stimulated neutrophils and macrophages (Steinbeck et al., 1992; Triantaphylidès and Havaux, 2009). Native compounds including flavins and NADH/NADPH inside the cell can function as photosensitizers and produce $^1O_2$ upon sunlight excitation, which has been linked to aging and cancer development in skin cells (Baier et al., 2006; Bäumler et al., 2012). Low levels of $^1O_2$ play an instructive role in intracellular signaling, such as promoting gene expression and triggering apoptosis (Anthony et al., 2005; Guo et al., 2010; Nam et al., 2013). However, high levels of $^1O_2$, especially the $^1O_2$ produced in vitro through photosensitization processes, can lead to excessive oxidation of biomolecules and even cell necrosis. Photosensitization or photodynamic processes require three key elements: photosensitizer, oxygen, and light (Fig. S1) (DeRosa and Crutchley, 2002). Actually, many photo-excitable molecules used in basic research, such as FITC and fluorescent proteins, are effective photosensitizers and can produce $^1O_2$ upon excitation.

Two unique features of $^1O_2$ are its short lifetime (μs) and its short working distance (nm), which make it effective in eliminating the function of specific proteins and cells with high temporal and spatial precision. In chromophore-assisted light inactivation, a fluorophore-tagged antibody recognizes and forms a complex with the target protein. Upon light excitation, an excessive

W. Gao and Z. Su contributed equally to this paper.
Correspondence to Lei Zhou: lzhou@vcu.edu

Abbreviations used in this paper: $^1O_2$, singlet oxygen; CNBD, cyclic nucleotide–binding domain; HCN, hyperpolarization-activated, cAMP-gated; I_h, hyperpolarization-activated current; I_{inst}, voltage-insensitive instantaneous current; LOV, light, oxygen, voltage; mHCN2, mouse HCN2; SOG, $^1O_2$ generator.

The Rockefeller University Press $30.00
J. Gen. Physiol. Vol. 143 No. 5 633–644
www.jgp.org/cgi/doi/10.1085/jgp.201311112

amount of $^1O_2$ is generated and inactivates the function of the protein in close proximity (Liao et al., 1994; Tour et al., 2003). Similarly in photodynamic therapy (PDT), light is guided to the target tissue to excite the pre-administered drugs (photosensitizers) to produce $^1O_2$, which eventually leads to the death of the target cells through a combination of apoptosis, necrosis, and acutely triggered local immune responses. The major advantage of PDT is the minimal side effects. PDT is a procedure approved by the US Food and Drug Administration for treating cancer and some other diseases (Agostinis et al., 2011).

However, in contrast to its application potential and physiological significance, little is known about $^1O_2$-mediated modification of biomacromolecules at the molecular level. Previous studies on $^1O_2$ mainly relied on cell and tissue preparations in the presence of complex intracellular signaling pathways. Numerous factors make $^1O_2$ a challenging research target: the volatile chemical nature of $^1O_2$; the wide range of target molecules; and the heterogeneous distributions of oxygen, photosensitizers, and quenchers (Schweitzer and Schmidt, 2003; Skovsen et al., 2005; Latch and McNeill, 2006; Pedersen et al., 2011). Isolated reports have addressed the effects of $^1O_2$ modification of channel and transporter proteins (Valenzeno and Tarr, 1991; Eisenman et al., 2007, 2009). Most of these studies used whole-cell preparations and applied nonspecific photosensitizers, such as rose bengal, to generate $^1O_2$. Thus, interactions between $^1O_2$ and lipid membranes or other membrane-affiliated elements could not be completely ruled out. Notably, all those studies required a long duration of light exposure—up to minutes or even longer—to produce observable effects, in contrast to the short lifetime of $^1O_2$ (µs). A well-defined and sensitive working model for studying $^1O_2$ modification is needed.

Here we report that hyperpolarization-activated, cAMP-gated (HCN) channels are sensitive to modification by photochemically generated $^1O_2$. HCN channels are involved in physiological functions including cardiac pacemaking, sensation of pain, learning, and memory (Robinson and Siegelbaum, 2003; Biel et al., 2009). HCN channels are tetrameric. Each subunit contains a transmembrane domain of six α helices (S1–S6), homologous to that of voltage-gated potassium channels, and the cyclic nucleotide–binding domain (CNBD) in the C terminus of the channel (Robinson and Siegelbaum, 2003; Biel et al., 2009). In the transmembrane domain, S4 contains multiple positively charged residues and functions as the voltage sensor for membrane hyperpolarization. Intracellular cAMP directly binds to the channel and increases current amplitude, shifts channel opening to less negative potentials, and slows down channel deactivation. cAMP-dependent gating in HCN channels contributes to the storage of working memory in the prefrontal cortex, the maintenance of heart rate at the resting level, and the sensation of pain (Nolan et al., 2003; Wang et al., 2007; Baruscotti et al., 2011). In addition to the hyperpolarization-activated current (I_h), HCN channels also conduct the voltage-insensitive instantaneous current (I_{inst}), although its molecular nature is not clear (Proenza et al., 2002; Mistrík et al., 2006; Proenza and Yellen, 2006). It was reported that I_h and I_{inst} could be conducted by two distinct populations of HCN channels that are not in rapid equilibrium (Proenza and Yellen, 2006).

The dual regulation of HCN channels by voltage and ligand provides a unique opportunity to study $^1O_2$ modification of membrane proteins. In our previous studies, we have used fluorescent cAMP analogues as a reporter to address the dynamic interaction between cAMP and the whole channel (Wu et al., 2011, 2012). Using 8-NBD-cAMP as the marker, we discovered that channels in the open state have an increased binding affinity for cAMP, and residues near the activation gate in S6 remotely control ligand binding. During these studies we noticed that applying high concentrations of fluorescein-cAMP (8-fluo-cAMP or FITC-cAMP) resulted in interesting changes to HCN function. Following this lead, we identified $^1O_2$ as the central player. Intriguingly, $^1O_2$ modification of the HCN channel is state dependent and depends on a critical histidine residue near the activation gate.

MATERIALS AND METHODS

Functional expression of HCN channels in *Xenopus laevis* oocytes

The DNA plasmid containing the sequence of WT mouse HCN2 (mHCN2) channel was provided by S. Siegelbaum (Columbia University, New York, NY). The HCN2-SOG and HCN2-EGFP constructs were made by inserting the DNA sequence encoding $^1O_2$ generator (SOG) or EGFP at the C terminus of the CNBD through the BsmI cut site, flanked by the CNBD and the downstream sequence of the mHCN2 channel (Figs. S2 and S3). The H434A mutation was introduced by a two-step PCR method. DNA plasmids were linearized by SphI and purified by phenol-chloroform extraction. mMessage machine (Ambion) was used to make cRNA. 40–50 ng cRNA was injected into each oocyte at stage VI. Injected cells were cultured between 16 and 18°C for 2–4 d before experiments.

Electrophysiology and optical setup

We used symmetrical solutions during patch-clamp recording in the inside-out configuration. The solution contained 110 mM KCl, 1 mM EDTA, and 10 mM HEPES, pH 7.4 adjusted by KOH. To measure ion selectivity, K^+ ions in the bath solution, which faced the intracellular side of the channel, were replaced by Na^+. All experiments were performed at room temperature. Current traces were amplified by a patch-clamp amplifier (model 2400; A-M Systems) and digitized by a Digidata 1440 (Axon Instruments). Voltage-clamp and laser-pulse protocols are illustrated in the figures. Typically the membrane potential was held at −40 mV. Hyperpolarizing voltage steps were applied every 15 s.

We calculated the percentage of I_{inst} based on the following equation:

$$I^i_{inst}(\%) = \frac{I^i_{inst} - I^0_{inst}}{I_{MAX}} \times 100,$$

where I_{inst} is the instantaneous current measured just after the hyperpolarizing voltage step, i is the stimulation index (episode number), I^0_{inst} is the instantaneous current before laser treatment, and I_{max} is the peak current measured near the end of the hyperpolarizing voltage step before laser treatment and includes both I_h and I_{inst}. We used a single-exponential equation to fit the tail current measured at −40 mV. Leak current was not subtracted from the recordings. To determine the $V_{1/2}$ values, a series of hyperpolarizing voltage steps was applied to activate the channel. Tail currents were measured at −40 mV, and the amplitudes were fitted with the Boltzmann equation.

The ratio of permeability for Na^+ and K^+ ions was calculated based on the value of the reversal potential and the Goldman–Hodgkin–Katz equation:

$$\frac{P_{Na}}{P_K} = \frac{\exp^{\frac{E_{REV}}{RT/F}} \cdot [K]i - [K]o}{[Na]o - \exp^{\frac{E_{REV}}{RT/F}} \cdot [Na]i},$$

where E_{REV} represents the reversal potential, and [X]o and [X]i represent the ion concentrations in the pipette and in the bath, respectively.

The setup was based upon a microscope (IX71; Olympus) equipped with a 100× oil-immersion objective (NA 1.25; Olympus Plan). A 473- or a 532-nm diode-pumped, solid-state laser was used as the excitation light source. The following filter set was used to collect the fluorescence signal from FITC, EGFP, and

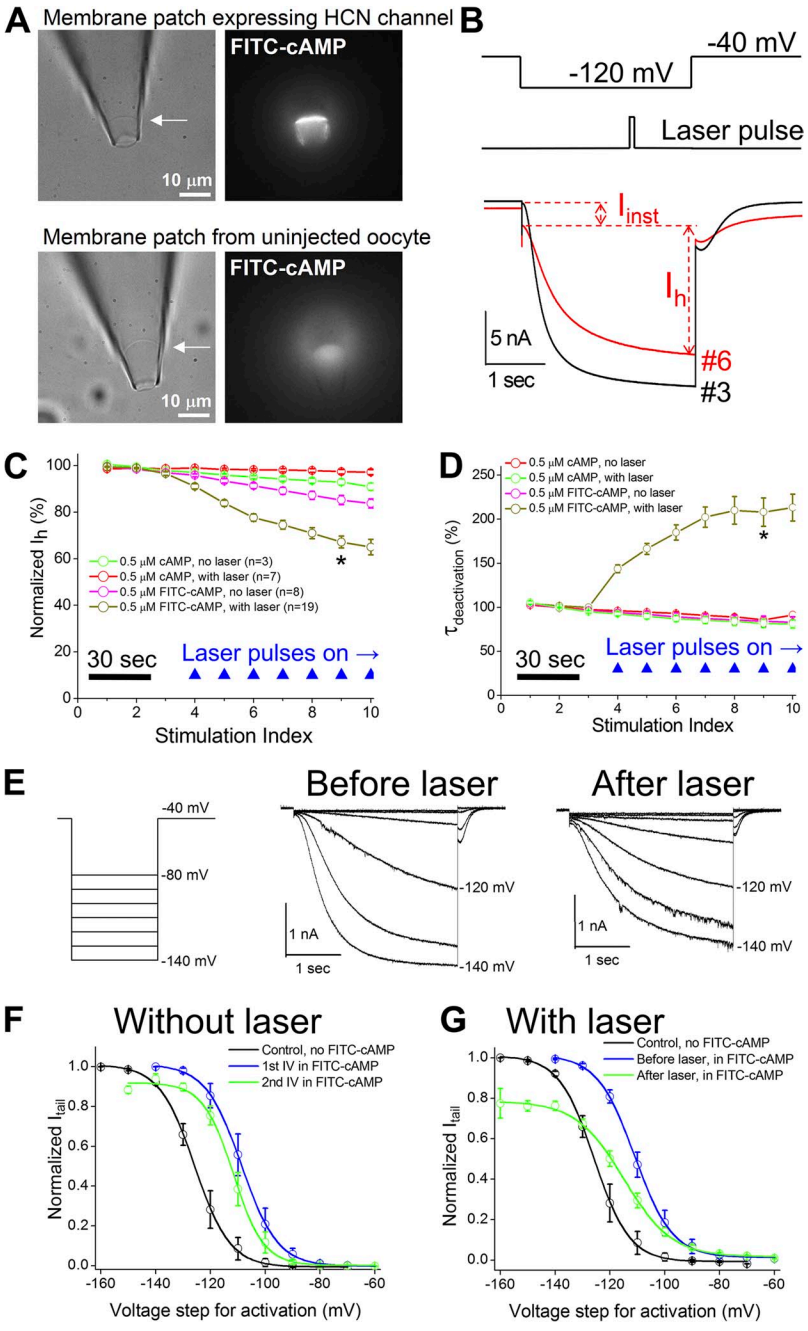

Figure 1. Effects on I_h current by photodynamic transformation. (A) Bright field (left) and fluorescence (right) images of a membrane patch expressing mHCN2 channels. Bottom pictures show a membrane patch from an uninjected cell. 0.5 μM FITC-cAMP was applied to the bath. (B; top) The voltage protocol for channel activation and the timing of 100-msec laser pulse. (Bottom) Representative current traces before (no. 3 in C) and after the application of laser pulses (nos. 6 and 9 in C). (C) Normalized I_h amplitude versus stimulation index. Voltage step was delivered every 15 s. (D) Normalized time constant of deactivation. *, $P < 0.05$ in C and D. (E; left) The voltage protocol for collecting I-V curve. (Middle) Current traces before the laser treatment. (Right) Current traces after the laser treatment. (F) I-V curves without laser treatment. The $V_{1/2}$ values are −126.7 ± 3.2 mV ($n = 8$; control without cAMP), −109.4 ± 2.6 mV (first I-V in 0.5 μM FITC-cAMP), and −112.5 ± 2.4 mV (second I-V in 0.5 μM FITC-cAMP). The averaged shift in $V_{1/2}$ is −3.1 ± 1.7 mV ($n = 7$) and not significant (one-way repeated measures ANOVA). (G) I-V curve with laser treatment. The $V_{1/2}$ values are −114.6 ± 1.6 mV (I-V in 0.5 μM FITC-cAMP before laser) and −120.4 ± 1.2 mV (I-V in 0.5 μM FITC-cAMP after laser treatments). The averaged shift in $V_{1/2}$ is −5.8 ± 0.8 mV ($n = 6$) and significant.

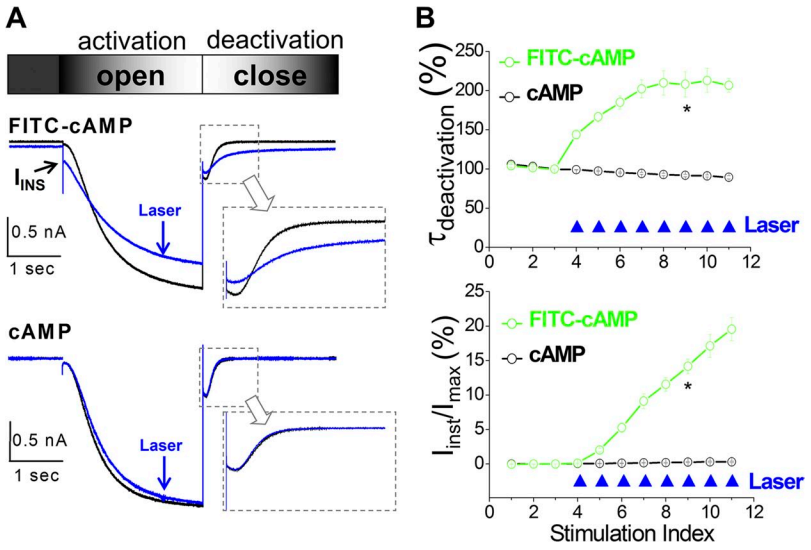

Figure 2. Photodynamic transformation slows down channel deactivation and enhances voltage-insensitive I_{inst}. (A) Current traces before (black; no. 3 in B) and after (blue; no. 7 in B) laser treatments. Arrow indicates I_{inst}. Gray arrows point out close-up view over the current traces during channel deactivation. (B) Percentage of I_{inst} (top) or time constant of channel deactivation (bottom) versus episode number. Laser pulses (filled blue triangle) were given every 15 s after the third episode. FITC-cAMP, n = 19; cAMP, n = 7. *, P < 0.05.

SOG: exciter, D480/30; dichroic mirror, DC505LP; emitter, D510LP. The intensity of the laser light applied to the membrane patch was estimated to be ∼350 mW/cm^2. Optical signals were detected by an EMCCD camera (Cascade 1K; Photometrics). The laser light source, the CCD camera exposure time, and the amplifier for patch-clamp recording were synchronized by transistor–transistor logic signals. Fluorescence images were analyzed with ImageJ software (Schneider et al., 2012). The TurboReg program

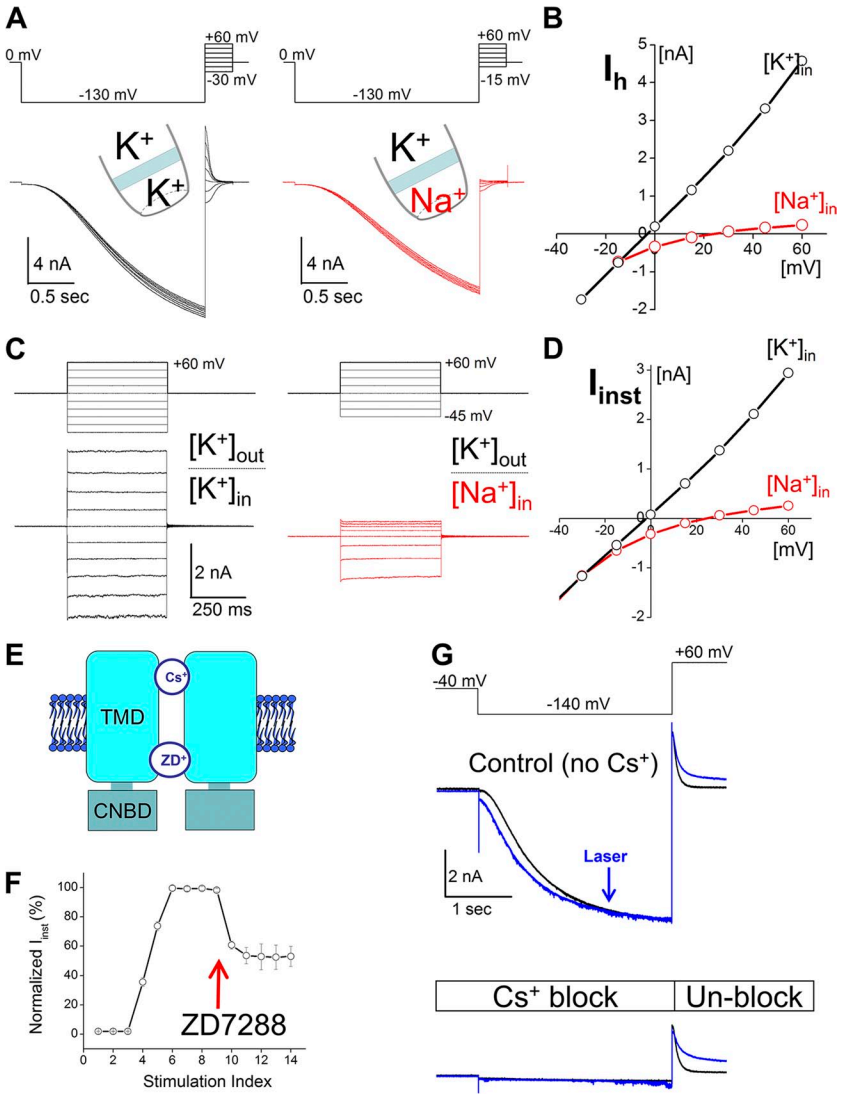

Figure 3. Photochemically generated I_{inst} has key biophysical features of canonical HCN channel. (A) Voltage protocol (top) and current traces for measuring pK^+/pNa^+ of I_h current. (B) I-V curves of I_h current. (C) Voltage protocols (top) and current traces of I_{inst}. (D) I-V curves of I_{inst}. (E) ZD7288 and Cs^+ interact with different regions in the HCN pore. (F) I_{inst} was generated by applying laser pulses (nos. 3–5). 60 µM ZD7288 was added to the bath solution after number 9. (G) 2 mM Cs^+ was added to the pipette solution. A voltage step to +60 mV released the Cs^+ block. Current traces: black, control; blue, after three laser pulses. Current traces in A–C were measured in the absence of ligands (cAMP or FITC-cAMP). 0.5 µM FITC-cAMP was present in F and G.

was used for image alignment. The fluorescent cAMP analogue, FITC-cAMP (8-fluo-cAMP), was obtained from Biolog. The stock solution of FITC-cAMP (1 mM, dissolved in ddH_2O) was kept frozen at −20°C. TROLOX was from Sigma-Aldrich. ZD7288 was from Tocris Bioscience.

Data analysis

Summarized data are presented as mean ± SEM. The number of experiments is indicated by *n*. One-way ANOVA (or one-way repeated measures ANOVA for the shift in $V_{1/2}$), followed by Tukey's post-hoc test, was used to evaluate data groups. P-values of <0.05 were considered significant and are indicated by an asterisk in the figures.

Online supplemental material

Fig. S1 shows working models for $^1O_2$ modification of HCN channel. Figs. S2 and S3 show the DNA and protein sequences of mHCN2-EGFP and mHCN2-SOG constructs. Fig. S4 shows decreases of I_h under different conditions. Fig. S5 shows the current trace at the moment when the laser pulse was applied. Fig. S6 shows that cAMP increases I_{inst}, and the negative control is shown in Fig. S7. Fig. S8 shows the results with mHCN2-EGFP as a negative control. Fig. S9 shows the results with rose bengal as the photosensitizer. Figs. S10 and S11 illustrate basic biophysical properties of the mHCN2/H434A mutant channel. Fig. S12 shows that the decrease of I_h amplitude in the mHCN2/H434A mutant channel was more dramatic than that in the WT channel. Fig. S13 shows the photodynamic transformation of the HCN channel with 2-ms laser pulses. The online supplemental material is available at http://www.jgp.org/cgi/content/full/jgp.201311112/DC1.

RESULTS

Photodynamic transformation of the mHCN2 channel

We performed experiments on a setup that enables simultaneous electrical recording of channel activity and optical detection of associated fluorescence signals (Wu et al., 2011). To prevent the interference from intracellular signal transduction pathways, we used a cell-free system and studied the channels expressed on a membrane patch held within the patch-clamp recording pipette in the inside-out configuration. To increase the spatial specificity of the photodynamic transformation, we used FITC-cAMP that specifically binds to the HCN channel on the cell membrane as the photosensitizer. Using uninjected oocytes as a negative control, we confirmed the specific interaction between FITC-cAMP and HCN channels (Fig. 1 A).

In the presence of 0.5 µM FITC-cAMP, a series of laser pulses applied during channel activation (473 nm, 100 msec, 1 pulse/episode) introduced significant functional changes in the mHCN2 channel (Fig. 1 B). Laser pulses significantly reduced the amplitude of the I_h current, slowed down channel deactivation, and enhanced the voltage-insensitive component (I_{inst}). First, we asked whether the changes in I_h after laser treatment are related to I_h rundown, which is a known phenomenon and reflected in both the reduction in current amplitude and the negative shift in the channel activation (I-V) curve. As a negative control, the same concentration of cAMP was applied to the patch. During the 3-min recording period, the reduction in I_h was minimal and less than ∼10% with laser pulses (Fig. 1, C and D, green trace). In contrast, I_h was reduced by ∼40% in the presence of FITC-cAMP and with laser pulses. Without laser treatment, applying FITC-cAMP led to a reduction in I_h, which was probably caused by the excitation of the fluorophore by ambient light. Further

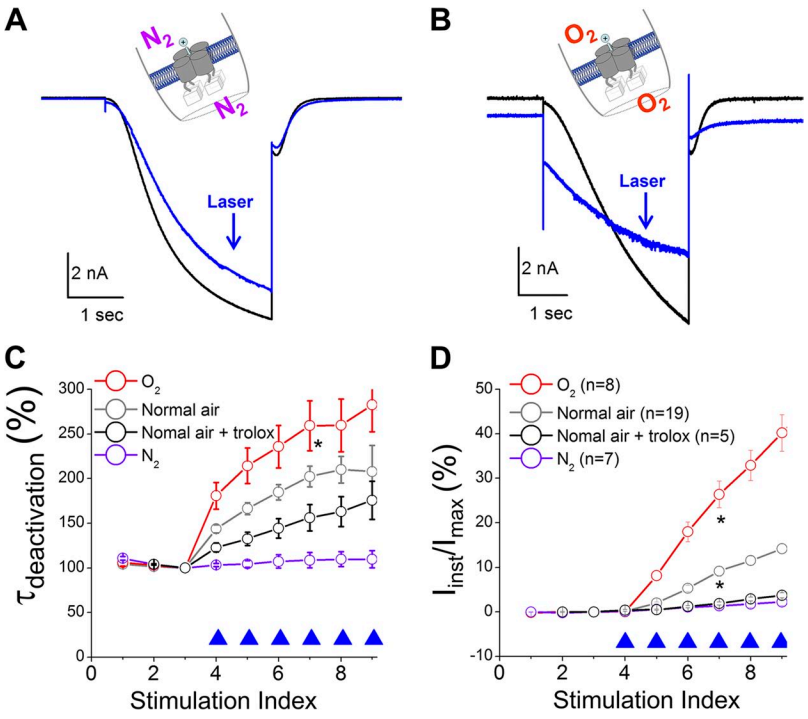

Figure 4. Photochemical transformation of the HCN channel is oxygen dependent. Solutions used in the experiments were degassed and then purged with pure N_2 or O_2. (A and B) Current traces before (black; no. 3 in C and D) and after laser pulses (blue; no. 8 in C and D). *, the group of O_2 is significantly different from the data groups of Normal air + trolox and N_2 (one-way ANOVA). (C and D) $\tau_{deactivation}$ or percentage of I_{inst} versus episode number. 0.5 µM FITC-cAMP was applied to the bath solution. *, the groups of O2 and normal air are significantly different from the other two data groups.

control experiments involving two other constructs were performed under different conditions (Fig. S4). Collectively, these results suggest that the photodynamic transformation of HCN channels is an active process and distinct from their rundown. Moreover, we studied hyperpolarization-dependent channel activation by measuring the I-V curve (Fig. 1 E). After adding FITC-cAMP to the bath, we collected an I-V curve as the first control and then applied two to four laser pulses before collecting the second I-V curve. Compared with the I-V curves collected without laser treatment, the photodynamic process decreased the maximal current amplitude and slightly shifted the I-V curve toward negative potentials (Fig. 1, F and G). Notably, for an HCN channel with a slow gating kinetics, it is known that the duration of voltage command affects the I-V curve and slight slowdown in activation could lead to a negative shift in $V_{1/2}$.

To quantify the changes in the amplitude of I_{inst} and the kinetics of channel deactivation, we calculated the percentage of I_{inst} in the total current and measured the time constant of channel deactivation (Fig. 2). The slowdown in channel deactivation occurred immediately after the delivery of the first laser pulse and reached a plateau after four to six pulses, whereas I_{inst} did not reach a plateau (Fig. S5). The "use-dependent" increase in I_{inst} could be related to the fact that after laser treatment the channel closed so slowly that a substantial amount of channels remained open, even until the next voltage stimulation step.

To confirm that the I_{inst} after laser treatment was carried by HCN channels but not related to nonspecific damage to the membrane patch, we characterized the biophysical properties of I_{inst} and compared them with those of the I_h current (Fig. 3). We started from ion selectivity because HCN channels have a distinctive mixed conductivity for K^+ and Na^+ ions. The ratio of permeability to K and Na is ~3:1. We first measured the relative permeability of the I_h current as a positive control. We separately applied solutions containing either K^+ or Na^+ to the intracellular side (Fig. 3 A). Based on the reversal potential, we determined P_K/P_{Na} of the I_h conductance to be 3.61 ± 0.21 (n = 3; Fig. 3 B). Next, we applied the photodynamic procedure to transform the channel and then determined P_K/P_{Na} to be 3.03 ± 0.22 (n = 7), which is not significantly different from that of I_h (one-way ANOVA) (Fig. 3, C and D). To further address the biophysical nature of I_{inst}, we asked whether I_{inst} could be

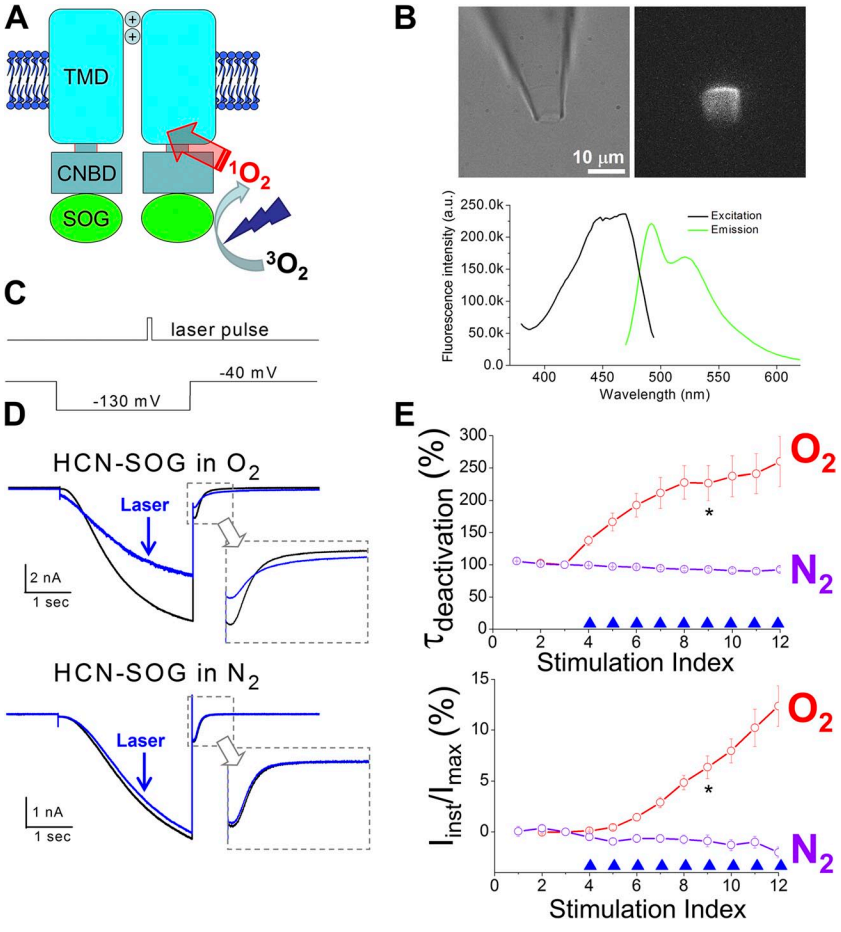

Figure 5. $^1O_2$ mediates photochemical transformation of the mHCN2 channel. (A) Construction of the HCN2-SOG fusion channel. (B; top) Bright field and fluorescence images of a membrane patch expressing HCN2-SOG channels. (Bottom) Excitation and emission spectra of purified mini-SOG protein. (C) Timing of the laser pulse and the voltage protocol. (D) Current traces before (black; no. 3 in E) and after (blue; no. 7 in E) laser treatments. (E) $\tau_{deactivation}$ or percentage of I_{inst} versus episode number. Neither cAMP nor FITC-cAMP was applied. *, P < 0.05.

blocked by known HCN channel blockers including ZD7288 and Cs^+ (Proenza and Yellen, 2006). Because two compounds block the channel from either side of the membrane, we separately tested them by applying 60 µM ZD7288 to the bath solution or 2 mM Cs^+ to the pipette solution. I_{inst} was significantly reduced by ZD7288 and completely blocked by Cs^+ (Fig. 3, E and F). Finally, we tested whether I_{inst} can be regulated by intracellular cAMP. After washing FITC-cAMP from the system, we applied 3 µM cAMP to the bath solution and observed a reversible increase in current amplitude (Figs. S6 and S7). These biophysical and pharmacological characterizations confirmed that the I_{inst} generated by the photochemical process carried key signatures of the HCN current.

$^1O_2$ is involved in the photochemical transformation of the mHCN2 channel

Next, we investigated the molecular basis of the photochemical transformation process. To further exclude nonspecific effects on the HCN channel by blue excitation light or green fluorescent emission, we used the HCN-EGFP fusion channel because EGFP and FITC share similar excitation and emission spectra (Fig. S8). Laser treatment had little effect on the channel. To test any potential effects by the green fluorescent light, we replaced the 473-nm laser with a green laser (532 nm) and directly illuminated the membrane patch. None of these manipulations produced any noticeable change in channel function. Collectively, it appears that the transformation of the HCN channel is through a photochemical process that involves the excitation of FITC.

Why does exciting FITC, but not EGFP, produce such dramatic effects on channel function? Compared with EGFP, FITC is known to have a higher quantum yield for generating $^1O_2$ (3 vs. 0.4%) (DeRosa and Crutchley, 2002; Jiménez-Banzo et al., 2008). To test the involvement of $^1O_2$, we applied 0.1 µM rose bengal, a widely used photosensitizer (Fig. S9), or 10 mM of free FITC to the intracellular side of the patch and indeed obtained similar observations. Then we asked whether the photodynamic process was sensitive to oxygen. We degassed the solutions used in the recordings and separately purged them with pure nitrogen or pure oxygen (Fig. 4, A and B). Impressively, removing oxygen from the solution effectively abolished the photochemical transformation of HCN function whereas, in contrast, the solutions purged with oxygen exaggerated the transformation effects. We also tested Trolox C, a known $^1O_2$ quencher (Ohara et al., 2009). As expected, 0.5 mM Trolox C (under normal air) suppressed the increases in $\tau_{deactivation}$ and I_{inst} (Fig. 4, C and D).

To further study the involvement of $^1O_2$, we engineered the recently developed mini-SOG protein to the C terminus of the HCN channel (Fig. 5, A and B). Mini-SOG was developed from the light, oxygen, voltage (LOV) domain of a plant protein. Mutations were introduced to increase the quantum yield of $^1O_2$ (up to 47%, ~20 times higher than that of ReAsh, a previously developed genetically targetable SOG) (Shu et al., 2011; Qi et al., 2012). In the absence of exogenous photosensitizers, light illumination of the HCN2-SOG channel reproduced the observations on the HCN2 channel in complex with FITC-cAMP (Fig. 5, C–E). Similarly, the photochemical transformation of the mHCN2-SOG channel was sensitive to oxygen.

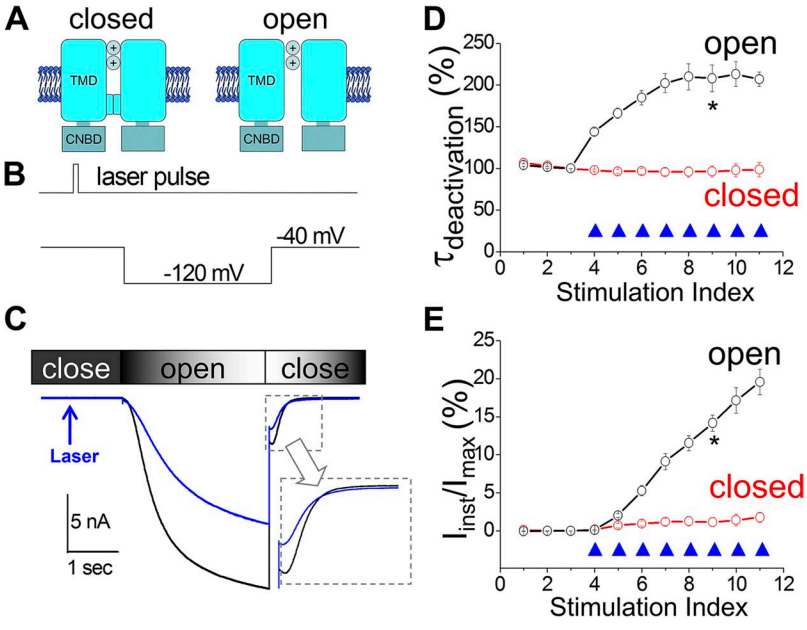

Figure 6. $^1O_2$ modification of the mHCN2 channel is state dependent. (A) Schematic drawings of closed and open channels. (B) Laser pulses were delivered preceding the hyperpolarization step. (C) Current traces before (black; no. 3 in D and E) and after (blue; no. 7 in D and E) laser treatments. (D and E) Normalized $\tau_{deactivation}$ or percentage of I_{inst} versus episode number. 0.5 µM FITC-cAMP was applied to the bath. *, $P < 0.05$.

State dependency in $^1O_2$ transformation of the mHCN2 channel and a critical histidine residue in the channel pore

The short duration of laser pulses (ms) used in our study enabled us to probe whether the timing of the $^1O_2$ modification, corresponding to different functional states of the channel, was a critical factor. We applied a light pulse preceding the hyperpolarizing voltage step, when most of the channels remained closed (Fig. 6, A and B). To our surprise, laser treatments of the closed channel reduced the I_h current amplitude but did not affect $\tau_{deactivation}$ or increase I_{inst} (Fig. 6, C–E). This result suggested that some effects of the transformation process, including increases in $\tau_{deactivation}$ and I_{inst}, are state dependent and require the channel to be in the open state when $^1O_2$ is released.

The above observation suggests that certain residue(s) might become more accessible to $^1O_2$ when the channel is in the open state. Following this insight, we tried to locate the residue(s) that underlies the $^1O_2$ modification effects. We focused on the regions that go through significant conformational changes during channel opening, such as the intracellular end of S6 where the activation gate was presumably located (del Camino et al., 2000; Shin et al., 2004; Prole and Yellen, 2006; Kwan et al., 2012; Wu et al., 2012). We discovered H434 to be important (Fig. 7 A). In the presence of FITC-cAMP, applying laser pulses negatively shifted the I-V curve of the mHCN2/H434A mutant channel and decreased the I_h amplitude (Figs. 7 B, S10, and S11). The negative shift in $V_{1/2}$ was about the same as the control (without laser pulses between two I-Vs), indicating a contribution by current rundown (Fig. 7 C). The decrease in the I_h amplitude of mHCN2/H434A is more pronounced than that of the WT channel (Fig. S12).

Importantly, alanine replacement of H434 effectively abolished the increases in $\tau_{deactivation}$ and I_{inst} upon light

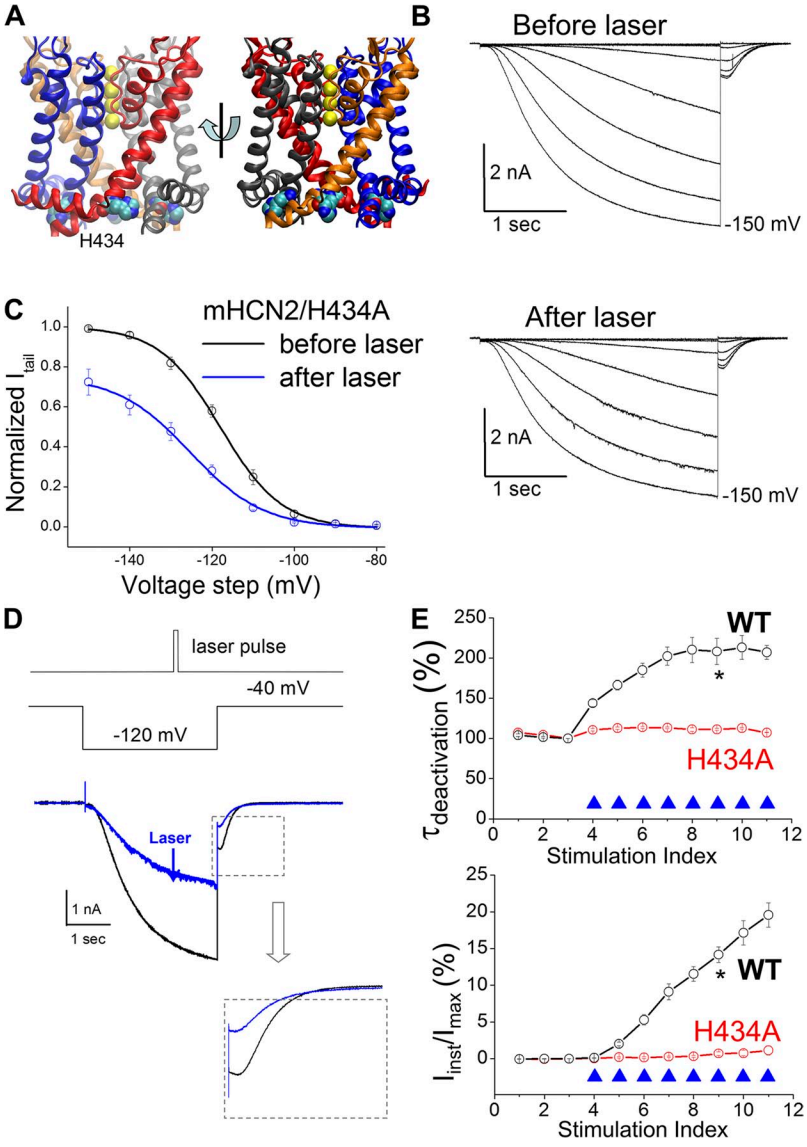

Figure 7. H434 is critical for $^1O_2$ modification of the mHCN2 channel. (A) Structure model of the mHCN2 pore (based on Kv1.2-2.1 chimeric structure) (Long et al., 2007). (B) Current traces of mHCN2/H434A mutant channel in the presence of 0.5 µM FITC-cAMP. A series of hyperpolarizing voltage steps in a −10-mV interval was used to activate I_h. (C) I-V curves of mHCN2/H434A before (black) and after (blue) laser treatment. Current amplitudes were normalized to the maximal level before laser treatment. $V_{1/2}$ values (with laser treatment) are −121.4 ± 1.7 mV (before laser in FITC-cAMP) and −129.7 ± 1.3 mV (after laser). The corresponding $\Delta V_{1/2}$ is −8.3 ± 2.0 mV (n = 7) and significant (one-way repeated measures ANOVA). As a control, the $V_{1/2}$ values in the presence of FITC-cAMP but without laser treatment are −119.6 ± 3.3 mV (first I-V) and −128.2 ± 4.1 mV (second I-V). The $\Delta V_{1/2}$ is −8.5 ± 1.6 mV (n = 8; significant). (D; top) Laser pulse. (Middle) Voltage protocol. (Bottom) Current traces before (black; no. 3 in D and E) and after (blue; no. 7 in D and E) laser treatments. (E) Normalized $\tau_{deactivation}$ or percentage of I_{inst} versus episode number. WT, n = 19; mHCN2/H434A, n = 13. *, P < 0.05.

stimulation (Fig. 7, D and E). These results support the working model that for channels in the open state, H434 becomes more accessible to $^1O_2$; subsequent modification of H434 leads to a delay in channel deactivation and the expression of the instantaneous HCN current (Fig. S1). In contrast, in the H434A mutant channel, $^1O_2$ becomes more abundant and modifications of other parts of the channel by $^1O_2$ might underlie the significant reduction in I_h current amplitude.

DISCUSSION

Here we report that HCN channels are very sensitive to photodynamic modification by $^1O_2$. FITC-cAMP or in-frame inserted SOG greatly increases the spatial specificity of $^1O_2$ production. In contrast with earlier studies that used second-to-minute long light illuminations, our study relied on millisecond light pulses, which exhibited significant changes in HCN channel function. Taking advantage of the short lifetime of $^1O_2$ and the slow gating kinetics of the HCN channel, we discovered that $^1O_2$ modification of HCN channels is state dependent and has distinct effects on channels in the open state compared with channels in the closed state. Following this lead, we identified a critical histidine residue at a critical region in S6. Impressively, replacing H434 abolished the effects of photodynamic transformation. Our study provides new insights into the instantaneous current conducted by the HCN channel and paves the way for further exploration of $^1O_2$ as an effective photonics tool.

HCN channels are known to conduct I_{inst}, but the physiological significance and the molecular basis have been unclear. The I_{inst} carried by HCN channels has been recorded from native cells, including neurons and cardiomyocytes, and heterologous expression systems (McCormick and Pape, 1990; Hagiwara et al., 1992; Irisawa et al., 1993; Maccaferri and McBain, 1996; Graf et al., 2001; Anderson et al., 2011). The I_{inst} conducted by HCN channels might have significant physiological consequences. On the one hand, it is known that nonphysiological negative potentials are required to activate the canonical I_h current, especially the currents carried by HCN2 and HCN4 channels. On the other hand, any compromise to HCN channel function, through either genetic or pharmacological approaches, consistently leads to a hyperpolarization shift of the resting membrane potential and an increase in the input resistance. I_{inst} might provide a hint for the resolution of this dilemma and some answers for exactly how HCN channels contribute to various physiological functions.

A molecular understanding of I_{inst} has been lacking. The most recent study reported that I_{inst} is conducted by a group of HCN channels that are distinct from the I_h-conducting channels (Proenza and Yellen, 2006). That observation is consistent with our current study in that the photodynamic transformation is an irreversible process, and the generated I_{inst} stayed at the same level during the recording period. Moreover, we observed similar results showing that I_{inst} can be up-regulated by cAMP and responds much faster to open channel blockers than I_h does. What is the molecular basis of I_{inst}? Our study suggests that modifications made to residues near the activation gate, such as H434, could slow down channel deactivation and produce I_{inst}. It is possible that under physiological conditions, certain residues including H434 are modified so that the channel's gate is decoupled from the gating machinery and remains open to produce I_{inst}. This is consistent with previous reports that the coupling between voltage sensor and gate in HCN channels is intrinsically weak compared with that in Kv channels (Bruening-Wright et al., 2007; Ryu and Yellen, 2012).

Our study revealed two major changes after photodynamic transformation: slowdown in channel deactivation and enhancement in I_{inst}. The two phenomena occurred concurrently and might even share the same molecular basis, but the connection between them requires further investigation. Delayed or incomplete deactivation should be able to directly contribute to the expression of I_{inst} by HCN channels, which had been seen in previous studies of a mutation in the S4–S5 linker that disrupts channel closing (Macri and Accili, 2004) and on the regulation of I_{inst} by intracellular chloride ions (Mistrík et al., 2006). As shown in Figs. 2 B and S5, it appears that the deactivation was slowed down after the first laser pulse (delivered in episode 4), but only in the next episode (5) could significant I_{inst} be detected. We kept the start-to-start interval between two episodes at 15 s, which is much longer than the cycle of membrane potential changes under physiological conditions when delayed deactivation will enhance the expression of I_{inst} upon repeated stimulations. Furthermore, the intrinsic connection between delayed deactivation and I_{inst} is supported by the observation that both were abolished when laser pulses were applied to the channels in the closed state or to the H434 mutant channel. However, we recognize the possibility that delayed deactivation and the generation of I_{inst} are not related. After photodynamic transformation, I_{inst} still exists even after a minute-long waiting period before the next hyperpolarizing stimulation. It is possible that modifications to H434 of different chemical natures are separately responsible for delayed or incomplete deactivation and the generation of I_{inst}. In the literature on I_{inst}, many studies do not report any changes in channel deactivation, although this could be caused by the fact that the I_h with delayed deactivation (and I_{inst}) only occupies a small fraction of the total current, so that the kinetics will not be affected macroscopically.

Our study only provided a peek into $^1O_2$ modification of proteins, which understandably is complicated. State-dependent photodynamic modification, most likely

through H434, suggests that the movement of $^1O_2$ and the modification of protein residues are not random processes. H434 is probably more accessible to $^1O_2$ when the channel is in the open state. This actually fits with a previous cysteine accessibility study reporting that the equivalent histidine in the spHCN channel (H462) is located approximately one to two α-helical turns above the critical region where four S6 α helices cross to form the channel gate (Rothberg et al., 2003). Because $^1O_2$ does not carry any extra electrostatic charges, the van der Waals force or steric clashes might be the dominant factor influencing the diffusion of $^1O_2$ through proteins. Moreover, we found that photochemical modification of the HCN channel reduced the I_h current amplitude and slightly shifted the channel activation curve toward negative potentials. The fact that I_h was reduced more in the mHCN2/434A mutant channel suggests that in the WT channel, H434 is dominant in the competition for photochemically generated $^1O_2$, but residues other than H434 might also be targeted by $^1O_2$, and the modification of those residues could underlie the decrease in I_h. Potential candidates include residues located in regions such as the S4–S5 linker or the intracellular ends of S5 and S6, which are known to be critical for channel function. In contrast to the decrease in I_h, the negative shift in $V_{1/2}$ upon photodynamic transformation was less significant for either WT or mHCN2/H434A mutant channels. Notably, because of the slow activation (seconds), the measurement of $V_{1/2}$ for HCN channels can be complicated by subtle changes in gating kinetics and the duration of voltage step applied. The effects on channel activation and the related shift in $V_{1/2}$ by photodynamic transformation require further investigation. FITC-cAMP also binds to other cyclic nucleotide–binding proteins including PKA and exchange proteins activated by cAMP, which should not be a major concern, as our experiments only involve isolated membrane patches in the inside-out configuration (Fig. 1 A). Nonspecific modifications could be largely excluded, as supported by the clear state dependency of $^1O_2$ modification of HCN channels and the results with the mHCN2/H434A mutant channel and the mHCN2-SOG channel.

The significance of the LOV domain in many different types of protein and the biological meaning of the sensitivity to $^1O_2$ remain to be clarified. The SOG protein used in this study was derived from the LOV domain of phototropin 2, a blue light photoreceptor from *Arabidopsis thaliana* (Shu et al., 2011). This domain was also found in the N terminus of the eag family (KCNH) of Kv channels (Morais Cabral et al., 1998; Haitin et al., 2013). Interestingly, both the LOV and the CNBD domains in KCNH channels lose the ability to interact with their corresponding cofactors, flavin mononucleotide and cyclic nucleotides, respectively, but they interact with each other to regulate channel function. The LOV domain has also been discovered in transcription factors that regulate circadian rhythms (Sassone-Corsi, 1998), some of which play a role in regulating $^1O_2$ signaling pathways (Metz et al., 2012). HCN channels share a similar topology with KCNH channels and do not contain the N-terminal LOV domain, but interestingly, they are very sensitive to regulation by $^1O_2$ generated by a mutated LOV domain. We anticipate that with a more powerful laser source and an ample supply of oxygen in the local microenvironment, it will be possible to push the time limit further to submilliseconds, a resolution that is essential for probing protein dynamics (Fig. S13). Further investigation of $^1O_2$ modification at the molecular level will provide insights into the role of $^1O_2$ as a signaling molecule and help establish $^1O_2$ as an effective photonics tool for biomedical research.

We thank Drs. Leon Avery and Roland Pittman for their suggestions and comments on this manuscript.

Q. Liu and L. Zhou are funded by startup funds from Virginia Commonwealth University and by the American Heart Association (grant 11BGIA7850004).

The authors declare no competing financial interests.

Edward N. Pugh Jr. served as editor.

Submitted: 27 September 2013
Accepted: 20 March 2014

REFERENCES

Agostinis, P., K. Berg, K.A. Cengel, T.H. Foster, A.W. Girotti, S.O. Gollnick, S.M. Hahn, M.R. Hamblin, A. Juzeniene, D. Kessel, et al. 2011. Photodynamic therapy of cancer: An update. *CA Cancer J. Clin.* 61:250–281. http://dx.doi.org/10.3322/caac.20114

Anderson, W.D., E.J. Galván, J.C. Mauna, E. Thiels, and G. Barrionuevo. 2011. Properties and functional implications of I_h in hippocampal area CA3 interneurons. *Pflugers Arch.* 462:895–912. http://dx.doi.org/10.1007/s00424-011-1025-3

Anthony, J.R., K.L. Warczak, and T.J. Donohue. 2005. A transcriptional response to singlet oxygen, a toxic byproduct of photosynthesis. *Proc. Natl. Acad. Sci. USA.* 102:6502–6507. http://dx.doi.org/10.1073/pnas.0502225102

Baier, J., T. Maisch, M. Maier, E. Engel, M. Landthaler, and W. Bäumler. 2006. Singlet oxygen generation by UVA light exposure of endogenous photosensitizers. *Biophys. J.* 91:1452–1459. http://dx.doi.org/10.1529/biophysj.106.082388

Baruscotti, M., A. Bucchi, C. Viscomi, G. Mandelli, G. Consalez, T. Gnecchi-Rusconi, N. Montano, K.R. Casali, S. Micheloni, A. Barbuti, and D. DiFrancesco. 2011. Deep bradycardia and heart block caused by inducible cardiac-specific knockout of the pacemaker channel gene *Hcn4*. *Proc. Natl. Acad. Sci. USA.* 108:1705–1710. http://dx.doi.org/10.1073/pnas.1010122108

Bäumler, W., J. Regensburger, A. Knak, A. Felgenträger, and T. Maisch. 2012. UVA and endogenous photosensitizers—the detection of singlet oxygen by its luminescence. *Photochem. Photobiol. Sci.* 11:107–117. http://dx.doi.org/10.1039/c1pp05142c

Biel, M., C. Wahl-Schott, S. Michalakis, and X. Zong. 2009. Hyperpolarization-activated cation channels: From genes to function. *Physiol. Rev.* 89:847–885. http://dx.doi.org/10.1152/physrev.00029.2008

Bruening-Wright, A., F. Elinder, and H.P. Larsson. 2007. Kinetic relationship between the voltage sensor and the activation gate

in spHCN channels. *J. Gen. Physiol.* 130:71–81. http://dx.doi.org/10.1085/jgp.200709769

del Camino, D., M. Holmgren, Y. Liu, and G. Yellen. 2000. Blocker protection in the pore of a voltage-gated K^+ channel and its structural implications. *Nature.* 403:321–325. http://dx.doi.org/10.1038/35002099

DeRosa, M.C., and R.J. Crutchley. 2002. Photosensitized singlet oxygen and its applications. *Coord. Chem. Rev.* 233–234:351–371. http://dx.doi.org/10.1016/S0010-8545(02)00034-6

Eisenman, L.N., H.J. Shu, G. Akk, C. Wang, B.D. Manion, G.J. Kress, A.S. Evers, J.H. Steinbach, D.F. Covey, C.F. Zorumski, and S. Mennerick. 2007. Anticonvulsant and anesthetic effects of a fluorescent neurosteroid analog activated by visible light. *Nat. Neurosci.* 10:523–530.

Eisenman, L.N., H.J. Shu, C. Wang, E. Aizenman, D.F. Covey, C.F. Zorumski, and S. Mennerick. 2009. NMDA potentiation by visible light in the presence of a fluorescent neurosteroid analogue. *J. Physiol.* 587:2937–2947.

Gracanin, M., C.L. Hawkins, D.I. Pattison, and M.J. Davies. 2009. Singlet-oxygen-mediated amino acid and protein oxidation: Formation of tryptophan peroxides and decomposition products. *Free Radic. Biol. Med.* 47:92–102. http://dx.doi.org/10.1016/j.freeradbiomed.2009.04.015

Graf, E.M., J.F. Heubach, and U. Ravens. 2001. The hyperpolarization-activated current I_f in ventricular myocytes of non-transgenic and β_2-adrenoceptor overexpressing mice. *Naunyn Schmiedebergs Arch. Pharmacol.* 364:131–139. http://dx.doi.org/10.1007/s002100100431

Guo, H.C., H.S. Qian, N.M. Idris, and Y. Zhang. 2010. Singlet oxygen-induced apoptosis of cancer cells using upconversion fluorescent nanoparticles as a carrier of photosensitizer. *Nanomedicine.* 6:486–495. http://dx.doi.org/10.1016/j.nano.2009.11.004

Hagiwara, N., H. Irisawa, H. Kasanuki, and S. Hosoda. 1992. Background current in sino-atrial node cells of the rabbit heart. *J. Physiol.* 448:53–72.

Haitin, Y., A.E. Carlson, and W.N. Zagotta. 2013. The structural mechanism of KCNH-channel regulation by the eag domain. *Nature.* 501:444–448.

Irisawa, H., H.F. Brown, and W. Giles. 1993. Cardiac pacemaking in the sinoatrial node. *Physiol. Rev.* 73:197–227.

Jiménez-Banzo, A., S. Nonell, J. Hofkens, and C. Flors. 2008. Singlet oxygen photosensitization by EGFP and its chromophore HBDI. *Biophys. J.* 94:168–172. http://dx.doi.org/10.1529/biophysj.107.107128

Kochevar, I.E. 2004. Singlet oxygen signaling: From intimate to global. *Sci. STKE.* 2004:pe7.

Kwan, D.C., D.L. Prole, and G. Yellen. 2012. Structural changes during HCN channel gating defined by high affinity metal bridges. *J. Gen. Physiol.* 140:279–291. http://dx.doi.org/10.1085/jgp.201210838

Latch, D.E., and K. McNeill. 2006. Microheterogeneity of singlet oxygen distributions in irradiated humic acid solutions. *Science.* 311:1743–1747. http://dx.doi.org/10.1126/science.1121636

Liao, J.C., J. Roider, and D.G. Jay. 1994. Chromophore-assisted laser inactivation of proteins is mediated by the photogeneration of free radicals. *Proc. Natl. Acad. Sci. USA.* 91:2659–2663. http://dx.doi.org/10.1073/pnas.91.7.2659

Long, S.B., X. Tao, E.B. Campbell, and R. MacKinnon. 2007. Atomic structure of a voltage-dependent K^+ channel in a lipid membrane-like environment. *Nature.* 450:376–382. http://dx.doi.org/10.1038/nature06265

Maccaferri, G., and C.J. McBain. 1996. The hyperpolarization-activated current (I_h) and its contribution to pacemaker activity in rat CA1 hippocampal stratum oriens-alveus interneurones. *J. Physiol.* 497:119–130.

Macri, V., and E.A. Accili. 2004. Structural elements of instantaneous and slow gating in hyperpolarization-activated cyclic nucleotide-gated channels. *J. Biol. Chem.* 279:16832–16846. http://dx.doi.org/10.1074/jbc.M400518200

McCormick, D.A., and H.C. Pape. 1990. Properties of a hyperpolarization-activated cation current and its role in rhythmic oscillation in thalamic relay neurones. *J. Physiol.* 431:291–318.

Metz, S., A. Jäger, and G. Klug. 2012. Role of a short light, oxygen, voltage (LOV) domain protein in blue light- and singlet oxygen-dependent gene regulation in *Rhodobacter sphaeroides*. *Microbiology.* 158:368–379. http://dx.doi.org/10.1099/mic.0.054700-0

Mistrík, P., A. Pfeifer, and M. Biel. 2006. The enhancement of HCN channel instantaneous current facilitated by slow deactivation is regulated by intracellular chloride concentration. *Pflugers Arch.* 452:718–727. http://dx.doi.org/10.1007/s00424-006-0095-0

Morais Cabral, J.H., A. Lee, S.L. Cohen, B.T. Chait, M. Li, and R. Mackinnon. 1998. Crystal structure and functional analysis of the HERG potassium channel N terminus: A eukaryotic PAS domain. *Cell.* 95:649–655. http://dx.doi.org/10.1016/S0092-8674(00)81635-9

Nam, T.W., E.C. Ziegelhoffer, R.A. Lemke, and T.J. Donohue. 2013. Proteins needed to activate a transcriptional response to the reactive oxygen species singlet oxygen. *MBio.* 4:e00541-12. http://dx.doi.org/10.1128/mBio.00541-12

Nolan, M.F., G. Malleret, K.H. Lee, E. Gibbs, J.T. Dudman, B. Santoro, D. Yin, R.F. Thompson, S.A. Siegelbaum, E.R. Kandel, and A. Morozov. 2003. The hyperpolarization-activated HCN1 channel is important for motor learning and neuronal integration by cerebellar Purkinje cells. *Cell.* 115:551–564. http://dx.doi.org/10.1016/S0092-8674(03)00884-5

Ogilby, P.R. 2010. Singlet oxygen: there is indeed something new under the sun. *Chem. Soc. Rev.* 39:3181–3209. http://dx.doi.org/10.1039/b926014p

Ohara, K., K. Kikuchi, T. Origuchi, and S. Nagaoka. 2009. Singlet oxygen quenching by trolox C in aqueous micelle solutions. *J. Photochem. Photobiol. B.* 97:132–137. http://dx.doi.org/10.1016/j.jphotobiol.2009.08.010

Pedersen, B.W., L.E. Sinks, T. Breitenbach, N.B. Schack, S.A. Vinogradov, and P.R. Ogilby. 2011. Single cell responses to spatially controlled photosensitized production of extracellular singlet oxygen. *Photochem. Photobiol.* 87:1077–1091. http://dx.doi.org/10.1111/j.1751-1097.2011.00951.x

Proenza, C., and G. Yellen. 2006. Distinct populations of HCN pacemaker channels produce voltage-dependent and voltage-independent currents. *J. Gen. Physiol.* 127:183–190. http://dx.doi.org/10.1085/jgp.200509389

Proenza, C., D. Angoli, E. Agranovich, V. Macri, and E.A. Accili. 2002. Pacemaker channels produce an instantaneous current. *J. Biol. Chem.* 277:5101–5109. http://dx.doi.org/10.1074/jbc.M106974200

Prole, D.L., and G. Yellen. 2006. Reversal of HCN channel voltage dependence via bridging of the S4–S5 linker and Post-S6. *J. Gen. Physiol.* 128:273–282. http://dx.doi.org/10.1085/jgp.200609590

Qi, Y.B., E.J. Garren, X. Shu, R.Y. Tsien, and Y. Jin. 2012. Photoinducible cell ablation in *Caenorhabditis elegans* using the genetically encoded singlet oxygen generating protein miniSOG. *Proc. Natl. Acad. Sci. USA.* 109:7499–7504. http://dx.doi.org/10.1073/pnas.1204096109

Robinson, R.B., and S.A. Siegelbaum. 2003. Hyperpolarization-activated cation currents: From molecules to physiological function. *Annu. Rev. Physiol.* 65:453–480. http://dx.doi.org/10.1146/annurev.physiol.65.092101.142734

Rothberg, B.S., K.S. Shin, and G. Yellen. 2003. Movements near the gate of a hyperpolarization-activated cation channel. *J. Gen. Physiol.* 122:501–510. http://dx.doi.org/10.1085/jgp.200308928

Ryu, S., and G. Yellen. 2012. Charge movement in gating-locked HCN channels reveals weak coupling of voltage sensors and

gate. *J. Gen. Physiol.* 140:469–479. http://dx.doi.org/10.1085/jgp.201210850

Sassone-Corsi, P. 1998. Molecular clocks: mastering time by gene regulation. *Nature.* 392:871–874. http://dx.doi.org/10.1038/31821

Schneider, C.A., W.S. Rasband, and K.W. Eliceiri. 2012. NIH Image to ImageJ: 25 years of image analysis. *Nat. Methods.* 9:671–675. http://dx.doi.org/10.1038/nmeth.2089

Schweitzer, C., and R. Schmidt. 2003. Physical mechanisms of generation and deactivation of singlet oxygen. *Chem. Rev.* 103:1685–1758. http://dx.doi.org/10.1021/cr010371d

Shin, K.S., C. Maertens, C. Proenza, B.S. Rothberg, and G. Yellen. 2004. Inactivation in HCN channels results from reclosure of the activation gate: Desensitization to voltage. *Neuron.* 41:737–744. http://dx.doi.org/10.1016/S0896-6273(04)00083-2

Shu, X., V. Lev-Ram, T.J. Deerinck, Y. Qi, E.B. Ramko, M.W. Davidson, Y. Jin, M.H. Ellisman, and R.Y. Tsien. 2011. A genetically encoded tag for correlated light and electron microscopy of intact cells, tissues, and organisms. *PLoS Biol.* 9:e1001041. http://dx.doi.org/10.1371/journal.pbio.1001041

Skovsen, E., J.W. Snyder, J.D. Lambert, and P.R. Ogilby. 2005. Lifetime and diffusion of singlet oxygen in a cell. *J. Phys. Chem. B.* 109:8570–8573. http://dx.doi.org/10.1021/jp051163i

Steinbeck, M.J., A.U. Khan, and M.J. Karnovsky. 1992. Intracellular singlet oxygen generation by phagocytosing neutrophils in response to particles coated with a chemical trap. *J. Biol. Chem.* 267:13425–13433.

Tour, O., R.M. Meijer, D.A. Zacharias, S.R. Adams, and R.Y. Tsien. 2003. Genetically targeted chromophore-assisted light inactivation. *Nat. Biotechnol.* 21:1505–1508. http://dx.doi.org/10.1038/nbt914

Triantaphylidès, C., and M. Havaux. 2009. Singlet oxygen in plants: production, detoxification and signaling. *Trends Plant Sci.* 14:219–228. http://dx.doi.org/10.1016/j.tplants.2009.01.008

Valenzeno, D.P., and M. Tarr. 1991. Membrane photomodification of cardiac myocytes: Potassium and leakage currents. *Photochem. Photobiol.* 53:195–201. http://dx.doi.org/10.1111/j.1751-1097.1991.tb03923.x

Wang, M., B.P. Ramos, C.D. Paspalas, Y. Shu, A. Simen, A. Duque, S. Vijayraghavan, A. Brennan, A. Dudley, E. Nou, et al. 2007. α2A-Adrenoceptors strengthen working memory networks by inhibiting cAMP-HCN channel signaling in prefrontal cortex. *Cell.* 129:397–410. http://dx.doi.org/10.1016/j.cell.2007.03.015

Wu, S., Z.V. Vysotskaya, X. Xu, C. Xie, Q. Liu, and L. Zhou. 2011. State-dependent cAMP binding to functioning HCN channels studied by patch-clamp fluorometry. *Biophys. J.* 100:1226–1232. http://dx.doi.org/10.1016/j.bpj.2011.01.034

Wu, S., W. Gao, C. Xie, X. Xu, C. Vorvis, F. Marni, A.R. Hackett, Q. Liu, and L. Zhou. 2012. Inner activation gate in S6 contributes to the state-dependent binding of cAMP in full-length HCN2 channel. *J. Gen. Physiol.* 140:29–39. http://dx.doi.org/10.1085/jgp.201110749